scientific reports

Check for updates

OPEN

Tumor budding and poorly differentiated clusters as a biological continuum in colorectal cancer invasion and prognosis

Tariq Sami Haddad[1]✉, John-Melle Bokhorst[1], Luuk van den Dobbelsteen[1], Sonay K. Öztürk[1], Elias Baumann[2], Shannon van Vliet[1], Kiek Verrijp[1], Nigel B Jamieson[3], Colin Wood[3], Martin D. Berger[4], Richard Kirsch[5], Marco Aben[1], Natasja Rutgers[1], Hideki Ueno[6], Francesco Ciompi[1], Femke Simmer[1], Jeroen van der Laak[1], Alessandro Lugli[2], Inti Zlobec[2] & Iris Nagtegaal[1]✉

Tumor budding (TB) and poorly differentiated clusters (PDCs) are features of infiltrative growth patterns and powerful independent prognostic factors in colorectal cancer (CRC), yet the underlying biological mechanisms behind their role in CRC invasion is less understood. The aim of this study was to investigate the molecular background and prognostic role of tumor cluster size at the invasive margin (IM) of CRC, and determine whether a biological continuum between TB and PDCs exists. Using a combination of spatial transcriptomic and immunohistochemical (IHC) techniques, we demonstrated a biological continuum from larger to smaller tumor clusters, with TB possessing greater invasive potential than PDCs. We deployed artificial intelligence on a cohort of 1134 Stage I-III CRC resections to automatically detect nearly 400,000 isolated tumor cells/clusters of any particular size across the IM. We determined that 2-celled clusters were the most abundant feature at the IM, and the simultaneous assessment of TB and PDCs yielded a prognostic performance stronger than either independently. Our study provides a deeper understanding of the mechanisms behind CRC invasion while improving risk stratification for Stage I-III CRC.

The invasive margin (IM) of colorectal cancer (CRC) represents the front line of a tumor as it spreads into surrounding tissue. We know that the IM plays a critical role in cancer invasion and disease progression. The IM can be fairly heterogenous with both pushing border (PB) as well as infiltrative border configurations. It has been previously shown that infiltrative growth patterns contribute to a worse disease-free survival in comparison to pushing borders[1,2]Due to a growing body of evidence linking IM patterns with patient survival[3], further investigation is needed to elucidate the biological mechanisms behind the invasive potential of the CRC tumor front.

Within the IM, distinct morphological features of cancer cell dissociation are represented by tumor budding (TB) and poorly differentiated clusters (PDCs). TB is defined as isolated cancer cells or cell clusters of < 5 cells located at the IM[4]. TB has been firmly established as a powerful independent predictor of lymph node metastasis, disease recurrence, and cancer-related death in CRC[5]TB has been incorporated into the World Health Organization Classification of Digestive System Tumours (2019)[6]and international CRC reporting protocols such as the International Collaboration on Cancer Reporting[7]PDCs are defined as isolated tumor clusters ≥ 5 cells without glandular formation[8]Several studies have demonstrated that PDCs are independently associated with poor outcomes[9]Novel grading systems combining TB and PDCs have shown that their combination is at least equivalent to their separate assessment[10].

TB and PDCs, despite the arbitrary cut-off of 5 cells, may be considered as different points of a biological continuum[9]Studies investigating the relation of TB and PDCs with the expression of epithelial-mesenchymal-transition (EMT) related markers, determined that TB and PDCs represent different manifestations of EMT,

[1]Radboud University Medical Center, Nijmegen, Netherlands. [2]Institute of Tissue Medicine and Pathology, University of Bern, Bern, Switzerland. [3]Wolfson Wohl Cancer Research Centre, School of Cancer Sciences, University of Glasgow, Glasgow, UK. [4]Department of Medical Oncology, Inselspital, Bern University Hospital, University of Bern, Bern, Switzerland. [5]Mt. Sinai Hospital, Toronto, Canada. [6]National Defense Medical College, Saitama, Japan. ✉email: tariq.haddad@radboudumc.nl; iris.nagtegaal@radboudumc.nl

with TB appearing to be closer to complete EMT than PDCs[11,12] Using a limited panel of characterization markers, there is yet to be a study which molecularly interrogates the concept of a biological continuum at the IM using a comprehensive spatial transcriptomic profiling of TB, PDC, and PB regions to elucidate mechanisms of CRC invasion.

Through the efforts of the International Tumor Budding consortium (ITB), an effective AI model for automated detection of TB in H&E whole slide images (WSIs) has been developed and validated in large series of CRC cases[13] By using the algorithm to detect isolated single tumor cells and cell clusters of any particular size, this is the first study to quantify nearly 400,000 single tumor cells/cell clusters across the IM of more than 1100 CRC cases. We determine cellular abundances of TB and PDCs and establish correlations with disease-free survival (DFS). We investigate whether the size of TB and PDCs plays a role in CRC prognostication and link these findings with our transcriptomic analysis to draw conclusions as to whether a biological continuum between PDCs and TB exists, and the role tumor clusters play in cancer invasion.

Materials and methods
Cohorts/Study populations
A cohort of 1134 primary tumors from patients with pTNM stage I-III CRC who did not receive neoadjuvant treatment was established by the IBC and used for the digital assessment and quantification of TB and PDCs using automated detection. The cohort is comprised of 163 cases from Switzerland, 601 cases from the Netherlands, and 370 cases from Canada. This study also included separately resection material from 20 cases at the Radboud University Medical Center (RadboudUMC) where TB, PDC and PB regions were identified and processed for spatial transcriptomic and immunohistochemical (IHC) analyses. Pathologists (SKO, IDN) were guided and selected regions based on a review of cases according to the International Tumor Budding Concensus Congress (ITBCC) 2016 guidelines[4]and using the formal definition of PDCs[8] This study was approved by ethical review boards at each center (approval numbers 2017 − 01803, 2017–3603, and REB17-0054-E). During their cancer treatment, patients provided informed consent, acknowledging that left-over tissue material could be used for research, and at that time, they expressed no objections to such use. All methods were performed in accordance with the relevant guidelines and regulations.

Digital assessment
TB and PDCs were assessed using a deep learning network for the automated detection of TB in H&E whole-slide images[13]The algorithm was used to detect all isolated tumor cells/cell clusters ranging in size from 1 to 10 cells. For each of the 1134 cases, an invasive margin of 1000 μm was determined using an IM detection algorithm[13] (Fig. 1A). All tumor cells/clusters ≤10 cells were quantified across the entire IM. All tumor cells/clusters from 1 to 4 cells were categorized as TB. All tumor clusters ranging from 5 to 10 cells were categorized as PDCs. TB was scored automatically for each case analogous to ITBCC guidelines[4]A TB hotspot of 0.785 mm^{2}was determined using a hotspot detection algorithm[13] The number of TB within the hotspot was determined to produce a TB score (Fig. 1B). The ITBCC cut-off of 10 buds for high-grade TB was used to distinguish between low and high-grade TB[4]. For the scoring of PDCs, a PDC hotspot of 0.785 mm^2 was determined using the hotspot detection algorithm. The number of PDCs within the hotspot was determined to produce a PDC score (Fig. 1C). A cutoff of 10 PDCs was used to distinguish between low and high-grade PDCs according to the method of Ueno et al.[8]. Tiered scoring was also performed in the same manner as done for traditional TB and PDC scoring but with increasing the tumor cluster size cut-off incrementally. This means that scores using the hotspot detection algorithm[13]with a hotspot of 0.785 mm^2 were determined separately for only single tumor cells, ≤ 2 cells, ≤ 3 cells, ≤ 4 cells (TB), ≤ 5 cells, ≤ 6 cells, ≤ 7 cells, ≤ 8 cells, ≤ 9 cells and ≤10 cells. A cutoff of 10 tumor cells/clusters was used to distinguish between low and high-grade for tiered scoring as was done for TB and PDC scoring. The decision was made to limit the detection to clusters ≤10 cells as 10-celled clusters accounted for < 0.5% of all tumor cells/clusters quantified in the study. The coordinates for all hotspots were measured in order to determine whether two hotspots overlapped or not.

Digital Spatial profiling (DSP)
In order to characterize intratumoral heterogeneity of the IM, 8 tissue microarrays (TMAs) consisting of 28, 32, and 29 cores representing TB, PDCs, and PB regions, respectively, were constructed from formalin-fixed paraffin-embedded (FFPE) resection material of 20 heterogenous CRC primary tumor cases collected at the RadboudUMC (Table S1). Serial Sect. (4 μm) of the TMA blocks were cut and mounted onto glass slides. For each TMA, we performed DSP using the Nanostring GeoMx DSP platform (NanoString, Seattle, WA, USA) and Cancer Transcriptome Atlas (CTA, NanoString) RNA panel as previously published[14–16]Pathologists (SKO, IDN) pre-selected regions of interest (ROIs) in H&E stained serial sections and selected the same ROIs in pan-cytokeratin-positive DSP sections according to the ITBCC guidelines[4]and using the formal definition of PDCs[8]Serial TMA sections stained with H&E were scanned processed using the automated TB detection algorithm[13] The algorithm quantified all tumor cells/clusters ≤10 cells within the H&E ROIs. PB ROIs were determined as having no TB or PDCs (Fig. 2A). PDC ROIs were determined as having more than 50% PDCs (Fig. 2B). TB ROIs were determined as having more than 50% TBs (Fig. 2C). Tumor areas of interest (AOIs) within the ROIs were selected based on PanCK + staining. TME AOIs were selected as PanCK−. Only regions contained within the ROIs were utilized in our analyses (Fig. 2). Data was processed and normalized as previously published[16].

Immunohistochemistry (IHC)
Serial Sect. (4 μm) of the TMAs pertaining to the 20 heterogenous CRC primary tumor cases were stained using H&E, AE1/AE3, and FN1 as previously published[16]Slides were scanned using a P1000 (3DHistech, Budapest,
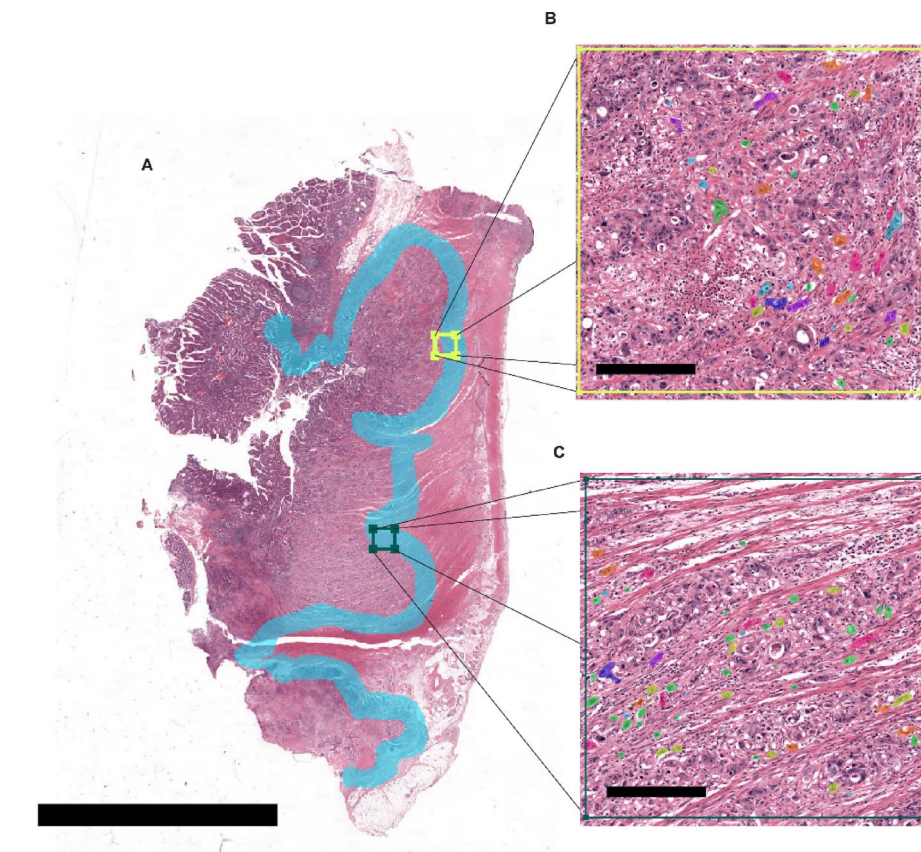
Fig. 1. Tumor Budding (TB) and Poorly Differentiated Cluster (PDC) assessment using automated detection in H&E using deep learning. (**A**) An H&E slide processed with the automated TB detection algorithm in H&E used to detect single tumor cells and tumor clusters ≤ 10 cells. A hotspot detection algorithm is used where densities of tumor buds and PDCs along the invasive front are determined. (**B**) Detection of tumor cells/clusters within the PDC hotspot (area = 0.785 mm[2]. Automatically detected tumor cells/clusters are denoted by the colored overlays. (**C**) Detection of tumor cells/clusters within the TB hotspot (area = 0.785 mm[2]. Automatically detected tumor cells/clusters are denoted with the colored overlays. Colored overlays are not indicative of size. The TB and PDC hotspots in this particular case do not overlap. (Scale bar = 10 mm; Inset = 250 μm).

Hungary). The same ROIs selected for the DSP experiments were selected in the IHC WSIs and only areas within the ROIs were included in our analyses. Stromal and epithelial FN1 expression in TB, PDC and PB regions were classified as previously published by two independent observers (TSH, LvdD) based on intensity as follows: 1, weak; 2, moderate; and 3, strong[16] No TB or PDC scoring was performed on IHC stained slides as the deep learning network only detects TB in H&E whole-slide images.

Statistical analyses

Statistical analyses were performed using R v4.2.0. Associations between TB, PDC as well as tiered scoring were evaluated using the Cox proportional hazards model. HR and 95% confidence intervals (CI) are reported. *P* values are reported and considered statistically significant when *P* < 0.05. Demographics and disease characteristics were compared by χ^2 and Kruskal-Wallis and when applicable. Transcriptomic data was preprocessed and normalized according to the GeomxTools 3.1.1 package developed by Nanostring (https://nanostring.com/resources/analyzing-geomx-ngs-rna-expression-datawith-geomxtools/). Differential gene expression across groups was analyzing using linear mixed-effect models[17] Spatial deconvolution analysis was performed using the Spatial Decon package (version 1.3) (https:github.com/Nanostring-Biostats/SpatialDecon/). Differentially expressed genes (DEGs) were defined as $\log_2$ fold = change > 0.5 and false discovery rate ≤ 0.05.

Results

Quantifying isolated tumor cells/clusters at the IM using automated detection

By automatically scoring TB and PDCs in H&E across the IM of 1134 pTNM Stage I-III cases, we quantified 378,412 single tumor cells and clusters ≤ 10 cells. Of all tumor cells/clusters quantified, single cells accounted for 20.1% and 2-celled clusters accounted for the largest percentage (44.4%) (Fig. 3A). Three-celled clusters accounted for 17.4% with a steadily decreasing percentage as the cluster size increased, with 10-celled clusters having a prevalence of only 0.4%. TB accounted for 90% of all single cells and cell clusters detected. When
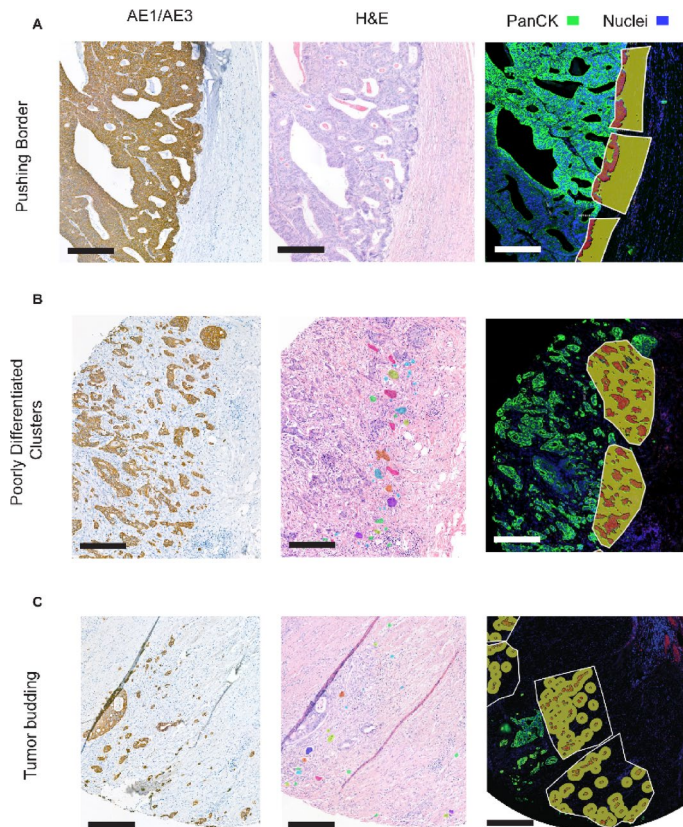
Fig. 2. Overview of Tumor Budding (TB), Poorly Differentiated Cluster (PDC), and Pushing Border (PB) regions. (**A**) (Left) A PB region from a pan-cytokeratin stained TMA serial section. (Center) The same PB region from an H&E stained serial section. (Right) The same PB region from a TMA serial section processed for Nanostring GeoMx Digital Spatial profiling (DSP). The section was stained with pan-cytokeratin (PanCK, green), CD45 (red) and DNA stainSyto13 (blue). The regions of interest (ROIs) are represented by the white irregular polygons. Within the ROIs, the areas of interest (AOIs) were selected based on segmentation of pan-cytokeratin staining. Tumor AOIs (all epithelium which is segmented red and contained within an ROI) are pan-cytokeratin +. Tumor microenvironment (TME) AOIs (all TME segmented yellow) surrounding the segmented epithelium within the ROI) are pan-cytokeratin –. Each AOI is considered a sample. (**B**) (Left) A PDC region from a pan-cytokeratin stained TMA serial section. (Center) The same PDC region from an H&E stained TMA serial section. Automatically detected tumor cells/clusters are denoted by the colored overlays. (Right) The same PDC region from a TMA serial section processed for DSP. (**C**) (Left) A TB region from a pan-cytokeratin stained TMA serial section. (Center) The same TB region from an H&E stained serial section. Automatically detected tumor cells/clusters are denoted by the colored overlays. (Right) The same TB region from a TMA serial section processed for DSP. Colored overlays are not indicative of size. (Scale bar = 250 μm).

breaking down the size percentages with regards to TB, 2-celled clusters accounted for nearly half (49.4%) of all TBs and 4-celled clusters were the least prevalent (9%) (Fig. 3B). Five-celled clusters comprised the majority of PDCs (41.7%) with a steadily decreasing prevalence as the cluster size increased to 10-celled clusters (4.3%) (Fig. 3C).

Hotspot overlap analysis of TB, PDCs, and tiered scoring system

When conducting the hotspot overlap analysis for TB, PDC, and tiered scoring on the H&E slides of the 1134 pTNM Stage I-III cases, we determined that TB and PDC hotspots overlapped in only 32.8% of cases suggesting that the highest densities of TBs and PDCs are often in differing areas of the IM (Fig. 3D). When comparing the hotspot of only single cells vs. groupings with increasing cluster size cut-off (single cells vs. ≤ 2 cells, single cells vs. ≤ 3 cells, etc.), the highest percentage overlap was between single cells vs. ≤ 2 cells (52.7%) and dropped to roughly 48% with gradually increasing cut-offs (Fig. 1D). When comparing the hotspot of ≤ 2 cells vs. all other groupings (≤ 2 cells vs. ≤ 3 cells, ≤ 2 cells vs. ≤ 4 cells, etc.), the highest percentage overlap was between ≤ 2 cells vs. ≤ 3 cells (81.3%) and leveled off at 75% as the cut-off increased (Fig. 3D). These findings suggest that single tumor cells are often more distributed across the IM compared with larger tumor clusters.

Analysis of tiered scoring and associations with DFS

In association with the tiered scoring performed on the H&E slides of the 1134 pTNM Stage I-III cases as described above, we conducted a cox regression analysis of tiered scoring ranging from a cut-off of only single
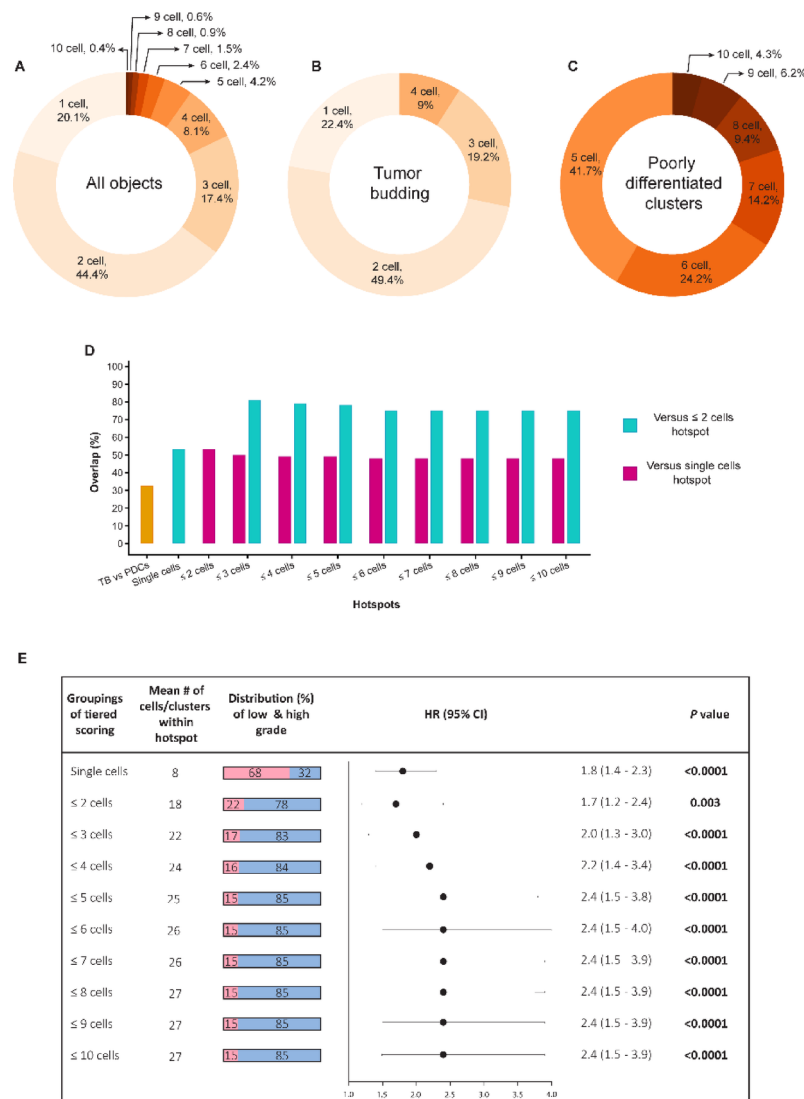
Fig. 3. Quantification of all tumor cells/clusters along the invasive front in a large series of colorectal cancer (CRC) cases. (**A**) Pie chart depicting percentages of tumor cells/clusters of a particular size out of all tumor cells/clusters ≤ 10 cells automatically detected across the entire invasive margin of all 1134 pTNM stage I-III CRC cases. (**B**) Pie chart depicting percentages of tumor cells/clusters of a particular size out of all tumor cells/clusters ≤ 4 cells detected and considered tumor budding (TB). (**C**) Pie chart depicting percentages of tumor cells/clusters of a particular size out of all tumor clusters detected with a size between 5 and 10 cells and considered poorly differentiated clusters (PDCs). (**D**) Percentage overlap of TB and PDC hotspots in all cases as well as the hotspots of increasing cluster size cut-off through the tiered scoring. (**E**) Table depicting the statistics of tiered scoring with cut-offs of only single cells and inclusion of cell clusters of incrementally increasing size. The mean number of tumor cells/clusters within a hotspot of each grouping, the distribution (%) of cases between low and high-grade groups, and hazard ratios for each grouping are depicted.

cells to ≤ 10 cells across the entire cohort to see how the inclusion of gradually larger tumor clusters being scored affects risk stratification and DFS. Using a cutoff of 10 to distinguish between low-risk and high-risk categories (as is done with traditional TB and PDC scoring), we saw that 68% of cases were considered low-risk when only single cells were scored (Fig. 3E). With the inclusion of 2-celled clusters, the distribution inverses with 78% of cases being considered high-risk (mean number of tumor cells/clusters within the hotspot increased from 8 to 18). After reaching a cutoff of ≤ 5 cells, the distribution of cases between the low-risk and high-risk categories stayed consistent at 15% and 85%, respectively. Scoring single cells only, patients in the high-risk category had nearly twice the risk compared to low-risk cases (Hazard Ratio (HR) 1.8, 95% CI 1.4–2.3; P value 0.0001). We observed a steady increase in the HR from ≤ 2 cells (HR 1.7, 95% CI 1.2–2.4; P value 0.003) to ≤ 5 cells (HR 2.4, 95% CI 1.5–4.0; P value < 0.0001) (Fig. 3E). At ≥ 5 cells, the risk plateaued and stayed consistently at HR 2.4. We therefore determined that for this cohort, there was no gain or loss in prognostic value with the inclusion of tumor clusters > 5 cells being scored.

Variables	Total (*n* = 1134)	Low-grade (*n* = 179)	High-grade (*n* = 955)	*P* value	Low-grade (*n* = 974)	High-grade (*n* = 160)	*P* value
Age (years), n (%)				0.99[c]			0.98[c]
< 70	605 (53.4)	96 (53.6)	509 (53.3)		519 (53.3)	86 (53.8)	
> 70	529 (46.6)	83 (46.4)	446 (46.7)		455 (46.7)	74 (46.2)	
Sex, n (%)				0.08[c]			0.47[c]
Male	583 (51.4)	81 (45.3)	502 (52.6)		496 (50.9)	87 (54.4)	
Female	551 (48.6)	98 (54.7)	453 (47.4)		478 (49.1)	73 (45.6)	
Tumor site, n (%)				0.03[c]			0.49[c]
Proximal	592 (52.2)	107 (59.8)	485 (50.8)		504 (51.7)	88 (55.0)	
Distal	542 (47.8)	72 (40.2)	470 (49.2)		470 (48.3)	72 (45.0)	
Tumor type, n (%)				< 0.0001[c]			0.18[c]
Adenocarcinoma	932 (82.2)	120 (67.0)	812 (85.0)		794 (81.5)	138 (86.3)	
Mucinous	202 (17.8)	59 (33.0)	143 (15.0)		180 (18.5)	22 (13.8)	
pT stage, n (%)				< 0.0001[c]			< 0.0001[c]
T1 + T2	239 (21.1)	58 (32.4)	181 (19.0)		227 (23.3)	12 (7.5)	
T3 + T4	895 (78.9)	121 (67.6)	774 (81.0)		747 (76.7)	148 (92.5)	
Node, n (%)				< 0.0001[c]			< 0.0001[c]
N0	678 (59.8)	144 (80.4)	534 (55.9)		614 (63.0)	64 (40.0)	
N+	456 (40.2)	35 (19.6)	421 (44.1)		360 (37.0)	96 (60.0)	
pTNM stage, n (%)				0.049[k]			0.049[k]
I	200 (17.6)	54 (30.2)	146 (15.3)		192 (19.7)	8 (5.0)	
II	478 (42.2)	90 (50.3)	388 (40.6)		422 (43.3)	56 (35.0)	
III	456 (40.2)	35 (19.6)	421 (44.1)		360 (37.0)	96 (60.0)	
MSI status, n (%)				0.0001[c]			0.09[c]
Proficient MMR	892 (78.7)	119 (66.5)	773 (80.9)		758 (77.8)	134 (83.8)	
Deficient MMR	206 (18.2)	50 (27.9)	156 (16.3)		185 (19.0)	21 (13.1)	
Unknown	36 (3.1)	10 (5.6)	26 (2.8)		31 (3.2)	5 (3.1)	
Differentiation, n (%)				0.95[c]			0.03[c]
Low grade	892 (78.7)	140 (78.2)	752 (78.7)		777 (79.8)	115 (71.9)	
High grade	242 (21.3)	39 (21.8)	203 (21.3)		197 (20.2)	45 (28.1)	
Lymphatic Invasion, n (%)				0.0002[c]			0.02[c]
No	616 (54.3)	125 (69.8)	491 (51.4)		561 (57.6)	55 (34.4)	
Yes	451 (39.8)	38 (21.2)	413 (43.2)		352 (36.1)	99 (61.9)	
Unk	67 (5.9)	16 (9.0)	51 (5.3)		61 (6.3)	6 (3.8)	
Perineural Invasion, n (%)				0.007[c]			0.02[c]
No	915 (80.7)	153 (85.5)	762 (79.8)		799 (82.0)	116 (72.5)	
Yes	133 (11.7)	9 (5.0)	124 (13.0)		99 (10.2)	34 (21.3)	
Unk	86 (7.6)	17 (9.5)	69 (7.2)		76 (7.8)	10 (6.3)	

Table 1. Clinicopathological Features of Cases Stratified by Tumor Budding (TB) and Poorly Differentiated Clusters (PDCs). [c]Chi-squared test; [k]Kruskall Wallis test; MSI = Microstaellite Instability; MMR = Mismatch repair.

Evaluation of TB, PDC scoring systems and associations with DFS

We proceeded to evaluate traditional TB and PDC scoring in H&E within the entire cohort. Clinicopathological features of the overall population and based on TB and PDC grading are shown in Table 1. Regarding TB, 15.8% cases were considered low-grade (Bd1-2) and 84.2% considered high-grade (Bd3). When scored for PDCs, the highest percentage of cases were considered low-grade (P1-2, 85.9%) compared to high-grade (P3, 14.1%). Cases with high-grade TB (Bd3) or high-grade PDCs (P3) were more frequently advanced stage disease compared to Bd1-2 or P1-2 cases respectively. This was accompanied by more lymphatic and perineural invasion. Bd1-2 tumors had relatively more MMR deficiency compared to Bd3 (*P* value = 0.0001). In turn, MMR-deficient tumors had fewer tumor buds than MMR-proficient tumors. Patients with Bd3 tumors had poorer DFS (HR 2.16, 95% CI 1.36–3.41; *P* value < 0.0001) in reference to Bd1-2 tumors compared to patients with P3 tumors (HR 1.53, 95% CI 1.30–2.12; *P* value = 0.01) and in reference to P1-2 tumors (Fig. 4A, B). We combined scores of TB and PDCs to see whether their synergistic performance was stronger than either independently (Fig. 4C). We observed that patients with high-risk cases (Bd3 & P3) had the worst DFS (HR 2.81, 95% CI 1.66–4.78; *P* value < 0.0001) in reference those with low-risk (Bd1-2 & P1-2) cases, and compared to Bd3 or P3 cases alone. Interestingly, we observed no cases across the entire cohort which were low-grade TB and high-grade PDCs (Bd1-2 & P3). The Intermediate-risk group (Bd3 & P1-2) (HR 2.04, 95% CI 1.28–3.24) had similar risk stratification to Bd3 alone group, suggesting that the low number or absence of PDCs scored in Bd3 cases has
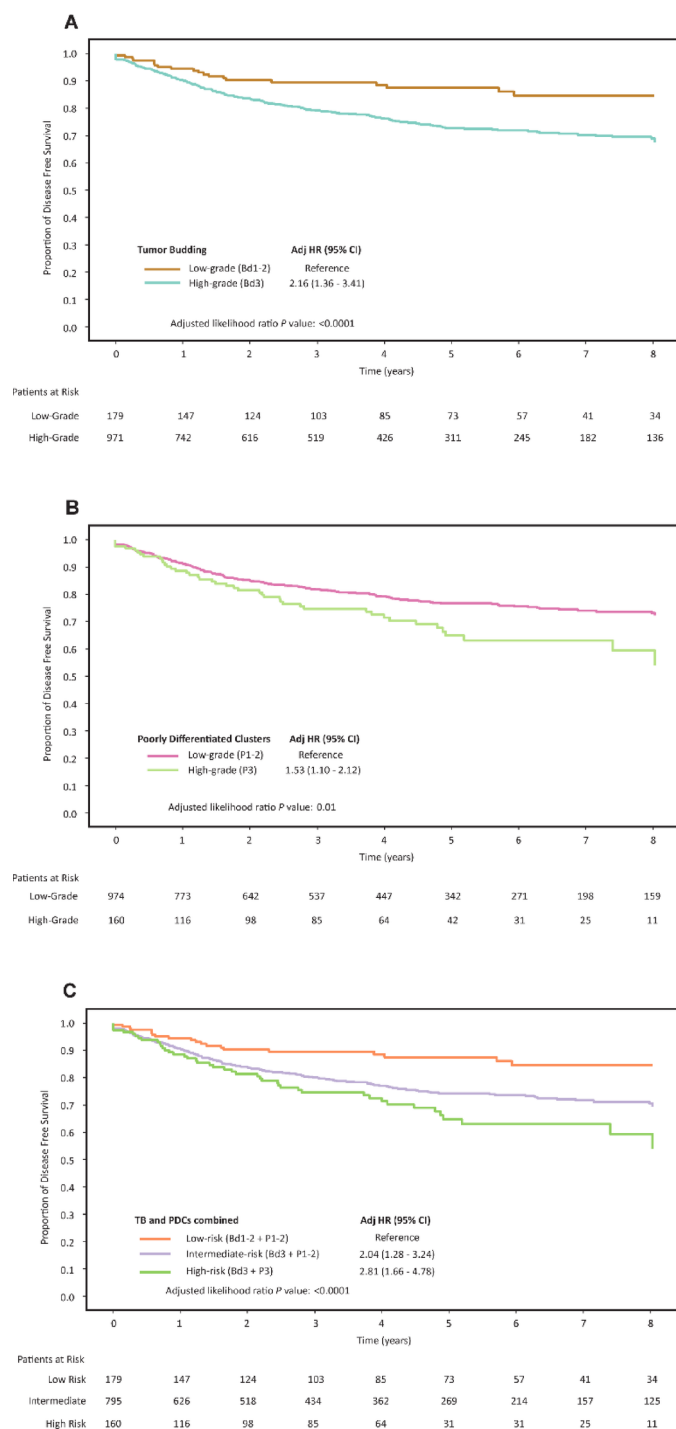
Fig. 4. Association of Tumor Budding (TB), Poorly Differentiated Clusters (PDCs), and their combined score with DFS for patients with Stage I-III colorectal cancer based on univariable analysis. (**A**) TB, (**B**) PDC, and (**C**) the combination of TB and PDC in overall cohort. HR, hazard ratio; CI, confidence interval.

nearly the same stratification compared to when PDCs were not scored. Non-existence of Bd3 & P1-2 cases suggests that large numbers of PDCs at the IM only exist with a high amount of TB.

Distinct transcriptomic profiles differentiate between PB, PDC, and TB regions with IHC validation

Having investigated the prognostic effects of TB, PDCs, single tumor cells and scores of increasing cluster size, we set out better understand the molecular background of tumor heterogeneity at the IM through the transcriptomic profiling of PB, PDC and TB regions within 20 heterogenous CRC cases using DSP. These regions presented distinct histology at the IM (Fig. 2A-C). Following preprocessing and normalization, we profiled the

expression of over 1,100 unique cancer related gene targets across 470 total samples, of which 235 represented the tumor and 235 the tumor microenvironment (TME). Of the 470 samples, 180 represented TB regions (90 tumor and 90 TME), 170 represented PDC regions (85 tumor and 85 TME), and 120 regions representing PB (60 tumor and 60 TME). When comparing PB and TB regions, we found 348 and 510 DEGs within the tumor and TME, respectively (Figure S1A, B and Table S1). In comparing PB and PDC regions, we found 131 and 35 statistically significant DEGs within the tumor and TME, respectively (Fig. 5A, B, and Table S1). Fibronectin 1 (*FN1*) and *SFRP2*, involved in migration and metastatic processes, were upregulated in PDCs regions along with matrix components such as *COL1 A1*, *COL3 A1*, and *COL1 A2*. When comparing PDC and TB regions, we found only 19 and 3 significant DEGs within the tumor and TME, respectively (Fig. 5C, D and Table S1). When comparing the tumor of PDC and TB regions, we found DEGs in TB regions involved with invasion and migration such as *FN1*, *COMP*, *SPP1*, as well as matrix components.

Spatial deconvolution of immune cell populations using DSP within the TME of PB, PDC and TB regions showed no significant differences in T-cell or B-cell populations (Fig. 5E). We observed significantly higher levels of macrophages in both TB and PDC regions compared to PB regions, as well as significantly higher levels of fibroblasts going from PB to PDC to TB regions (Fig. 5E).

To validate the transcriptomic upregulation of FN1, we performed FN1 IHC staining on TMA serial sections (Fig. 6A-C) of the 20 cases described above where DSP was performed. Based on the FN1 IHC stained slides, we observed significantly higher stromal FN1 expression in PDC compared to PB regions (Fig. 6D). There was no significant difference in stromal FN1 expression between PDC and TB regions. We observed significant differences in epithelial FN1 expression with significantly higher expression going from PB to PDC to TB regions (Fig. 6E). These findings correlated with transcriptomic *FN1* expression (Fig. 5A-D, Figure S1A, B, and Table S1).

Discussion

Through our investigation of TB and PDCs at the IM, we successfully demonstrated a biological continuum from larger to smaller tumor clusters and single tumor cells, with TB having more invasive potential than PDCs. We determined that 2-celled clusters are the most abundant feature at the IM, and a high number of PDCs did not exist without the presence of a high amount of TB. TB and PDC scores in combination yielded a prognostic performance stronger than either independently.

Two-celled clusters being the most abundant feature at the IM (44.4%) supports the idea of collective migration and that CRC invasion occurs more often in clusters rather than as individual tumor cells[18,19] CRC invasion may occur more often in smaller than larger clusters as mechanical confinement delimits tissue space and forces multicellular movement of epithelial cells between tissue surfaces[20] This may also explain why we did not observe an increased risk stratification with a cluster size cut-off beyond 5 cells (Fig. 3E). TB in relation with collective cell migration is also supported by multiple 3D studies observing TB as continuous finger-like extensions from the main tumor[21-23] With isolated single cell/cell cluster migration considered rare, CRC cell migration is more likely a combination of attenuated protrusions from the main tumor with occasional isolated cell clusters and least commonly single cells. This may also reflect a transitional state of CRC migration from projections to isolated tumor clusters/cells. It has been shown that mesenchymal single cells resemble leader cells during collective migration, suggesting the potential duality of single-celled TB observed in 2D as both mesenchymal single cells and more commonly leader cells in collective migration[24].

In the progression from PB to PDC to TB regions, we observed an upregulation of DEGs associated with the deposition of extracellular matrix (ECM), cancer invasion and migration. Increased deposition of ECM through an upregulation of *COL3 A1*, *COL5 A2*, and *COL6 A3* is associated with advanced staging, metastasis, and poor prognosis[25-27] An upregulation of *SFRP2* promotes therapeutic resistance in a damaged tumor microenvironment, with SFRP1/2-expressing cancer associated fibroblast populations supporting epithelial tumor progression[28,29] Overexpression of *LAMC2* in CRC is associated with poor prognosis by promoting cancer cell migration and invasion[30] Both *COMP* and *SPP1* promote malignant progression and metastasis through cytoskeletal remodeling and activating the EMT pathway[31-34].

The ECM undergoes continuous remodeling, a process regulated by matrix metalloproteinases (MMPs). Among them, *MMP9* plays a pivotal role in cleaving ECM proteins like collagen and elastin, thereby facilitating ECM turnover. Elevated *MMP9* expression was observed in TB regions compared to PDC regions (Fig. 5), and is often correlated with enhanced tumor invasion and metastasis in CRC, as *MMP9* upregulation contributes to degradation of the basement membrane and interstitial stroma, promoting cancer cell dissemination[35] There is also suggestion of a strong relationship between *MMP9* expression in TB and a more aggressive tumor phenotype[36] *MMP1* and *MMP11*, which were elevated in PDC regions compared to PB regions, are known to promote colorectal cancer cell migration[37,38] Our spatial deconvolution analysis revealed a significant increase in macrophages and fibroblasts in TB and PDC regions compared to PB regions, suggesting their role in ECM remodeling and tumor progression. Macrophages promote ECM degradation by secreting *MMP9* and enhance fibroblast activation via TGF-β, leading to increased collagen and *FN1* production[39,40] Similarly, fibroblasts, which were more abundant in TB and PDC regions, regulate ECM composition by secreting FN1 and collagen, contributing to ECM stiffness and tumor invasion[41].

Increased deposition of ECM is a hallmark of desmoplastic reaction (DR), referring to fibrotic tissue response surrounding invasive tumors and characterized by fibroblast proliferation. DR results in stromal fibrosis, which contributes to the structural integrity of the TME, influences tumor progression and is correlated to our findings of increased ECM deposition and presence of fibroblasts in TB regions. In CRC, the presence and maturity of DR at the invasive front has been linked to patient prognosis. Ueno et al. categorized DR in CRC to three patterns- mature, intermediate, and immature-based on histological features (keloid-like collagen and myxoid stroma), with immature DR having been associated with poorer outcomes[42] These findings highlight stromal fibrosis as a key factor in CRC progression.
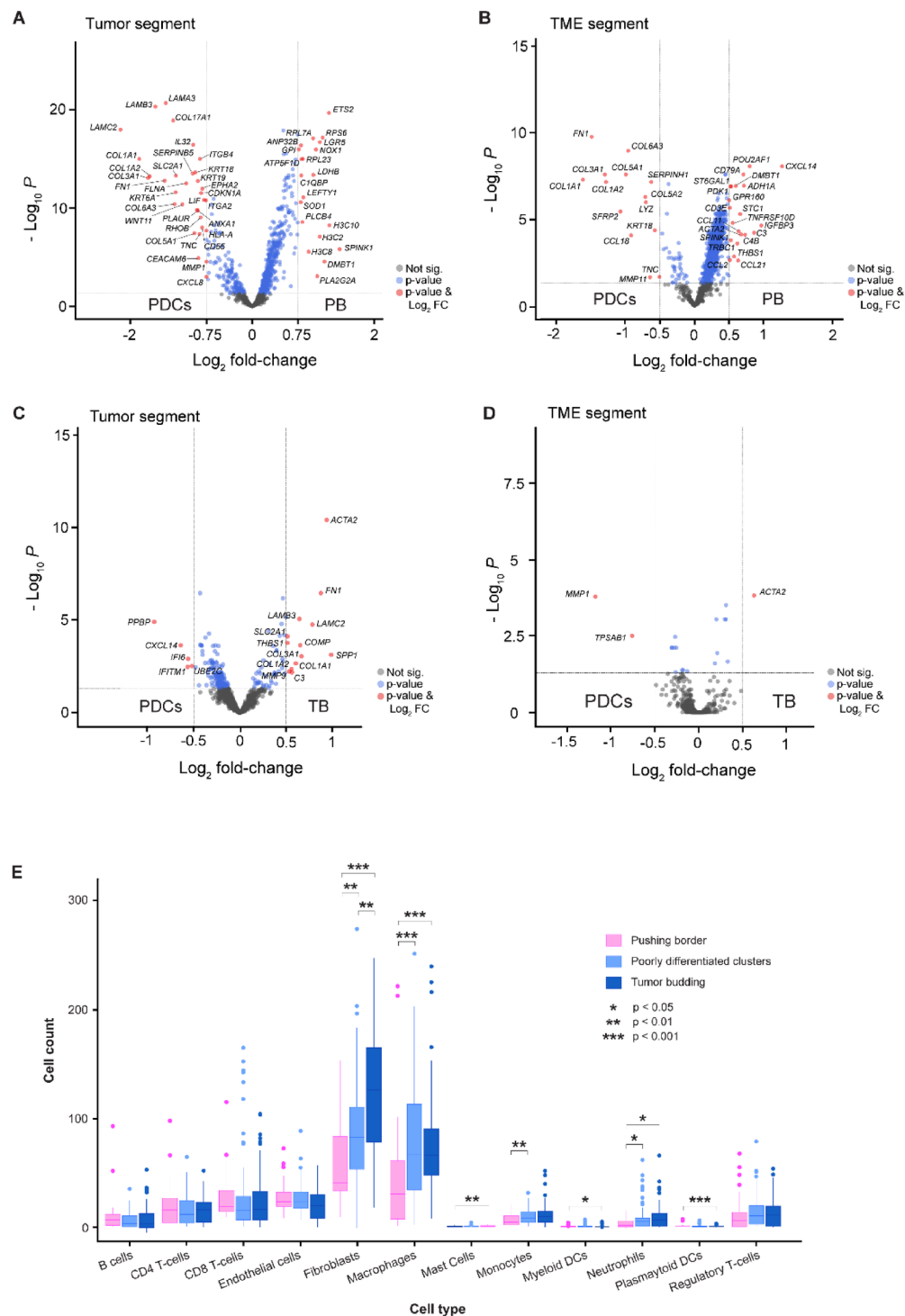
Fig. 5. Transcriptional profiles and Differentially Expressed Genes (DEG) between Tumor Budding (TB), Poorly Differentiated Clusters (PDC) and Pushing Border (PB) regions. DEGs between TB, PDC and PB regions using Nanostring GeoMx Digital Spatial Profiling (DSP). (**A**) Volcano plot demonstrating DEGs within the tumor area of 60 and 85 samples representing PB and PDC, respectively. X-axis represents -Log$_2$ fold change and Y-axis represents -Log$_{10}p$ value. (**B**) Volcano plot demonstrating DEGs within the tumor microenvironment (TME) of 60 and 85 samples representing PB and PDC, respectively. (**C**) Volcano plot demonstrating DEGs within the tumor area of 90 and 85 samples representing TB and PDC, respectively. (**D**) Volcano plot demonstrating DEGs within the TME of 90 and 85 samples representing TB and PDC, respectively. (**E**) Spatial deconvolution of immune cell populations within the TME of TB, PDC and PB regions, respectively. Statistical comparison done using a Wilcoxon test.
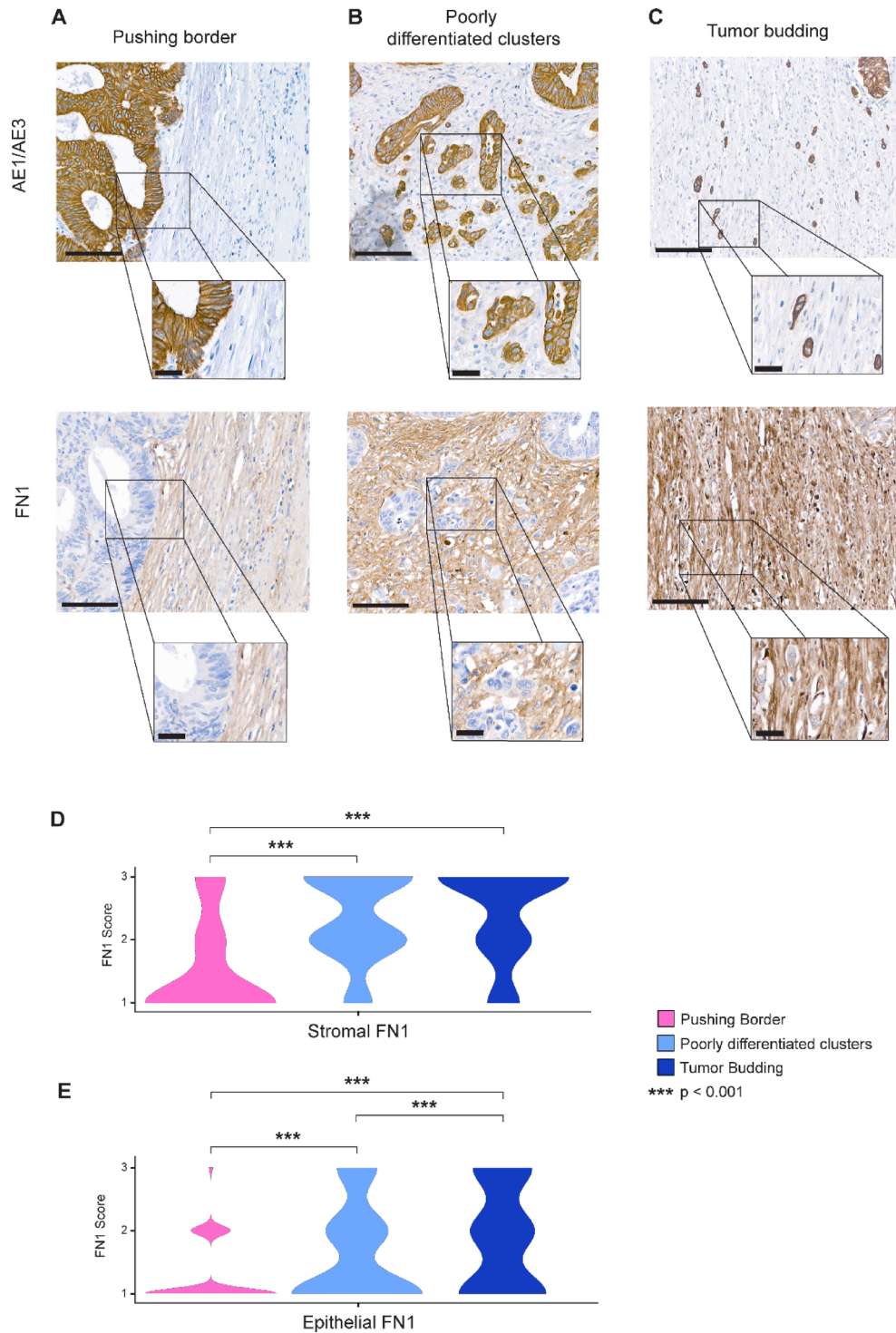
Fig. 6. Validation of transcriptomic expression using Immunohistochemistry (IHC). On TMA serial sections, pan-cytokeratin (AE1/AE3) and Fibronectin 1 (FN1) staining was performed for all Tumor Budding (TB), Poorly Differentiated Clusters (PDC), and Pushing Border (PB) regions. (**A**) The same representative PB region stained with (upper) AE1/AE3 and (lower) FN1. (**B**) The same representative PDC region stained with (upper) AE1/AE3 and (lower) FN1. (**C**) The same representative TB region stained with (upper) AE1/AE3 and (lower) FN1. (**D**) Violin plot showing stromal FN1 expression scored across all TB (dark blue), PDC (light blue), and PB (pink) regions ($p < 0.001$, T-test). (**E**) Violin plot showing epithelial FN1 expression scored across all TB (dark blue), PDC (light blue), and PB (pink) regions ($p < 0.001$, T-test). (Scale bar = 100 μm; Inset = 25 μm).

Budding regions are characterized by a phenotypic switch compared to the bulk by acquiring migratory characteristics, becoming EMT positive, and decreasing cell proliferation[16,43] FN1, of which we observed increased transcriptomic and protein expression of in TB regions compared to PDC and PB regions, is associated with an EMT response[44] In-vitro knockdown of *FN1* in CRC cell lines significantly inhibited invasion and cellular migration[44,45] Pavlic et al. showed that TB and PDCs are related to partial EMT, with TB being closer to complete EMT than PDCs[11] A mean decrease in Ki-67 labeling and higher nuclear β-catenin index was also observed in the progression from tumor core to PDCs to TB[12] Based on our findings, TB appears to possess greater invasive potential than PDCs which supports their role as leader cells during collective migration or mesenchymal single cells in CRC invasion. These findings also correlate with a higher prognostic value observed for TB compared to PDCs (Fig. 4).

Several studies have shown the independent prognostic strength of both TB and PDCs, with our findings supporting their clinical relevance in early-stage CRC[5,8,9,46–51] High-grade TB in early-stage CRC is a risk factor for LNM and may warrant radical surgery with lymph node dissection[3,5] Stage II CRC with high-grade TB is considered high-risk and patients may benefit from adjuvant therapy[3,5] PDCs are similarly predictive in stage II CRC as patients with high-grade PDC had a significantly worse 5-year DFS than patients with Stage III and low-grade PDC[52] These high-risk Stage II patients may benefit from adjuvant chemotherapy[9] PDC grade may also help guide post-operative surveillance of stage III patients[9].

Currently, TB and PDCs are assessed manually in diagnostic practice. Shivji et al. showed that the combination of TB and PDC into a single manual scoring system provides a risk stratification in CRC at least equivalent to that of TB and PDCs assessed individually[10] Manual scoring is time-consuming and often plagued by low interobserver agreement[46,53] AI models can serve to score TB and PDC more efficiently and reproducibly[13,54] The increased prognostic performance we observed by combining automated TB and PDC scores may be due in part to the assessment of multiple hotspot areas rather than one as only 32.8% of cases had overlapping hotspots (Fig. 3D). Considering this, it may be worth re-evaluating how TB and PDCs are scored and expanding beyond a single hotspot-based system. Automated detection allows for more complex assessment such as multiple hotspots or the entire IM which may give a more accurate assessment as to how aggressive a tumor actually is. Further studies are needed to determine whether TB and PDCs should be combined into a single scoring system as well as explore and evaluate new assessment strategies. Until then, we recommend that TB and PDCs be assessed simultaneously in routine diagnostics to improve risk stratification and help identify high-risk Stage I, II, and III cases which may benefit from radical resection, adjuvant therapy, or surveillance, respectively.

Our study utilizes a large, multicentric cohort of Stage I-III CRC cases. Limitations are that this study is retrospective and uses a deep learning algorithm which has not yet been implemented in routine diagnostic practice. This study also does not account for temporal changes as is inherent to histopathology, and investigates a single timepoint after the tumor has been excised.

In summary, our study provides evidence for the biological continuum of PDCs and TB as they represent different points of CRC invasion. TB has greater invasive potential and prognostic value than PDCs, with both showing significantly more invasive potential compared to PB regions. The prognostic performance of scoring TB and PDCs simultaneously provides strong evidence for their adoption into standard of care. The study also emphasizes the value of incorporating AI into diagnostic practice which can help optimize diagnostic assessment and benefit patients.

Data availability
The transcriptomics data presented in this study are available in the supplementary material.

References

1. Jass, J. R., Love, S. B. & Northover, J. M. A. A new prognostic classification of rectal cancer. *Lancet* **329**, 1303–1306 (1987).
2. Karamitopoulou, E. et al. Tumour border configuration in colorectal cancer: proposal for an alternative scoring system based on the percentage of infiltrating margin. *Histopathology* **67**, 464–473 (2015).
3. Zlobec, I., Berger, M. D. & Lugli, A. Tumour budding and its clinical implications in Gastrointestinal cancers. *Br. J. Cancer*. **123**, 700–708 (2020).
4. Lugli, A. et al. Recommendations for reporting tumor budding in colorectal cancer based on the international tumor budding consensus conference (ITBCC) 2016. *Mod. Pathol.* **30**, 1299–1311 (2017).
5. Lugli, A., Zlobec, I., Berger, M. D., Kirsch, R. & Nagtegaal, I. D. Tumour budding in solid cancers. *Nat. Reviews Clin. Oncol.* **18**, 101–115 (2020).
6. Board, W. C. o.T.E. *Digestive System Tumours: WHO Classification of Tumours*, Vol. 1, Edn. 5thWorld Health Orgn,. (2019).
7. Loughrey, M. B. et al. Colorectal Cancer Histopathology Reporting Guide. International Collaboration on Cancer ReportingSydney, Australia;. (2020).
8. Ueno, H. et al. New criteria for histologic grading of colorectal Cancer. *Am. J. Surg. Pathol.* **32** (2012).
9. Shivji, S., Conner, J., Barresi, V. & Kirsch, R. Poorly differentiated clusters in colorectal cancer: A current review and implications for future practice. *Histopathology* (2020).
10. Shivji, S. et al. A novel combined tumor Budding-Poorly differentiated clusters grading system predicts recurrence and survival in stage I-III colorectal Cancer. *Am. J. Surg. Pathol.* **46**, 1340–1351 (2022).
11. Pavlic, A. et al. Tumour budding and poorly differentiated clusters in colon cancer - different manifestations of partial epithelial-mesenchymal transition. *J. Pathol.* **258**, 278–288 (2022).
12. Hong, M., Kim, J. W., Shin, M. K. & Kim, B. C. Poorly differentiated clusters in colorectal adenocarcinomas share biological similarities with micropapillary patterns as well as tumor buds. *J. Korean Med. Sci.* **32**, 1595–1602 (2017).
13. Bokhorst, J. M. et al. Fully automated tumor bud assessment in hematoxylin and Eosin stained whole slide images of colorectal Cancer. *Mod. Pathol.*, 100233 (2023).

14. Zollinger, D. R., Lingle, S. E., Sorg, K., Beechem, J. M. & Merritt, C. R. GeoMx RNA assay: high multiplex, digital, Spatial analysis of RNA in FFPE tissue. *Methods Mol. Biol.* **2148**, 331–345 (2020).
15. Fisher, N. C. et al. Biological misinterpretation of transcriptional signatures in tumor samples can unknowingly undermine mechanistic Understanding and faithful alignment with preclinical data. *Clin. Cancer Res.* **28**, 4056–4069 (2022).
16. Haddad, T. S. et al. Pseudobudding: ruptured glands do not represent true tumor buds. *J. Pathol.* (2023).
17. Bates, D., Mächler, M., Bolker, B. & Walker, S. Fitting linear Mixed-Effects models using lme4. *J. Stat. Softw.* **67**, 1–48 (2015).
18. Friedl, P. & Alexander, S. Cancer invasion and the microenvironment: plasticity and reciprocity. *Cell* **147**, 992–1009 (2011).
19. Cheung, K. J., Gabrielson, E., Werb, Z. & Ewald, A. J. Collective invasion in breast cancer requires a conserved basal epithelial program. *Cell* **155**, 1639–1651 (2013).
20. Ilina, O. et al. Cell–cell adhesion and 3D matrix confinement determine jamming transitions in breast cancer invasion. *Nat. Cell. Biol.* **22**, 1103–1115 (2020).
21. Bronsert, P. et al. Cancer cell invasion and EMT marker expression: a three-dimensional study of the human cancer-host interface. *J. Pathol.* **234**, 410–422 (2014).
22. Yoshizawa, T. et al. Three-dimensional analysis of extrahepatic cholangiocarcinoma and tumor budding. *J. Pathol.* **251**, 400–410 (2020).
23. Lin, J. R. et al. Multiplexed 3D atlas of state transitions and immune interaction in colorectal cancer. *Cell* **186**, 363–381e319 (2023).
24. Parlani, M., Jorgez, C. & Friedl, P. Plasticity of cancer invasion and energy metabolism. *Trends Cell. Biol.* **33**, 388–402 (2023).
25. Liu, W., Li, L., Ye, H., Tao, H. & He, H. Role of COL6A3 in colorectal cancer. *Oncol. Rep.* **39**, 2527–2536 (2018).
26. Wang, J., Jiang, Y. H., Yang, P. Y. & Liu, F. Increased collagen type V alpha2 (COL5A2) in colorectal Cancer is associated with poor prognosis and tumor progression. *Onco Targets Ther.* **14**, 2991–3002 (2021).
27. Zhang, H. et al. Data mining-based study of collagen type III alpha 1 (COL3A1) prognostic value and immune exploration in pan-cancer. *Bioengineered* **12**, 3634–3646 (2021).
28. Kasashima, H. et al. Stromal SOX2 upregulation promotes tumorigenesis through the generation of a SFRP1/2-Expressing Cancer-Associated fibroblast population. *Dev. Cell.* **56**, 95–110e110 (2021).
29. Sun, Y. et al. SFRP2 augments WNT16B signaling to promote therapeutic resistance in the damaged tumor microenvironment. *Oncogene* **35**, 4321–4334 (2016).
30. Huang, D., Du, C., Ji, D., Xi, J. & Gu, J. Overexpression of LAMC2 predicts poor prognosis in colorectal cancer patients and promotes cancer cell proliferation, migration, and invasion. *Tumour Biol.* **39**, 1010428317705849 (2017).
31. Amilca-Seba, K. et al. Osteopontin (OPN/SPP1), a mediator of tumor progression, is regulated by the mesenchymal transcription factor Slug/SNAI2 in colorectal Cancer (CRC). *Cells* **11** (2022).
32. Xu, C. et al. SPP1, analyzed by bioinformatics methods, promotes the metastasis in colorectal cancer by activating EMT pathway. *Biomed. Pharmacother.* **91**, 1167–1177 (2017).
33. Qi, J. et al. Single-cell and Spatial analysis reveal interaction of FAP(+) fibroblasts and SPP1(+) macrophages in colorectal cancer. *Nat. Commun.* **13**, 1742 (2022).
34. Zhong, W. et al. Cartilage oligomeric matrix protein promotes epithelial-mesenchymal transition by interacting with Transgelin in colorectal Cancer. *Theranostics* **10**, 8790–8806 (2020).
35. Huang, H. Matrix Metalloproteinase-9 (MMP-9) as a Cancer biomarker and MMP-9 biosensors: recent advances. *Sens. (Basel Switzerland)* **18** (2018).
36. Guzińska-Ustymowicz, K. MMP-9 and cathepsin B expression in tumor budding as an indicator of a more aggressive phenotype of colorectal cancer (CRC). *Anticancer Res.* **26**, 1589–1594 (2006).
37. Pan, C. et al. Matrix metalloproteinase 11 promotes migration and invasion of colorectal Cancer by elevating slug protein. *Int. J. Med. Sci.* **21**, 2170–2188 (2024).
38. Wang, X., Liu, Y., Ding, Y. & Feng, G. CAMSAP2 promotes colorectal cancer cell migration and invasion through activation of JNK/c-Jun/MMP-1 signaling pathway. *Sci. Rep.* **12**, 16899 (2022).
39. Illemann, M. et al. MMP-9 is differentially expressed in primary human colorectal adenocarcinomas and their metastases. *Mol. Cancer Res.* **4**, 293–302 (2006).
40. Liu, C., Zhang, W., Wang, J., Si, T. & Xing, W. Tumor-associated macrophage-derived transforming growth factor-β promotes colorectal cancer progression through HIF1-TRIB3 signaling. *Cancer Sci.* **112**, 4198–4207 (2021).
41. Onfroy-Roy, L., Hamel, D., Malaquin, L. & Ferrand, A. Colon fibroblasts and inflammation: sparring partners in colorectal Cancer initiation?? *Cancers (Basel)* **13** (2021).
42. Ueno, H. et al. Histologic categorization of desmoplastic reaction: its relevance to the colorectal cancer microenvironment and prognosis. *Ann. Surg. Oncol.* **22**, 1504–1512 (2015).
43. De Smedt, L. et al. Expression profiling of budding cells in colorectal cancer reveals an EMT-like phenotype and molecular subtype switching. *Br. J. Cancer.* **116**, 58–65 (2017).
44. Park, J. & Schwarzbauer, J. E. Mammary epithelial cell interactions with fibronectin stimulate epithelial-mesenchymal transition. *Oncogene* **33**, 1649–1657 (2014).
45. Cai, X. et al. Down-regulation of FN1 inhibits colorectal carcinogenesis by suppressing proliferation, migration, and invasion. *J. Cell. Biochem.* **119**, 4717–4728 (2018).
46. Konishi, T. et al. Poorly differentiated clusters predict Colon cancer recurrence: an In-Depth comparative analysis of Invasive-Front prognostic markers. *Am. J. Surg. Pathol.* **42**, 705–714 (2018).
47. Ryan, É. et al. Tumor budding and PDC grade are stage independent predictors of clinical outcome in mismatch repair deficient colorectal Cancer. *Am. J. Surg. Pathol.* **42**, 60–68 (2018).
48. Lee, S. J. et al. The significance of tumor budding in T1 colorectal carcinoma: the most reliable predictor of lymph node metastasis especially in endoscopically resected T1 colorectal carcinoma. *Hum. Pathol.* **78**, 8–17 (2018).
49. Lee, V. W. K. & Chan, K. F. Tumor budding and poorly-differentiated cluster in prognostication in stage II colon cancer. *Pathol. Res. Pract.* **214**, 402–407 (2018).
50. Ammendola, S. et al. The presence of poorly differentiated clusters predicts survival in stage II colorectal cancer. *Virchows Arch.* **478**, 241–248 (2021).
51. Barresi, V., Bonetti, R., Ieni, L., Caruso, A., Tuccari, G. & R.A. & Poorly differentiated clusters: clinical impact in colorectal Cancer. *Clin. Colorectal Cancer.* **16**, 9–15 (2017).
52. Ueno, H. et al. Peritumoral deposits as an adverse prognostic indicator of colorectal cancer. *Am. J. Surg.* **207**, 70–77 (2014).
53. Bokhorst, J. M. et al. Assessment of individual tumor buds using keratin immunohistochemistry: moderate interobserver agreement suggests a role for machine learning. *Mod. Pathol.* **33**, 825–833 (2020).
54. Pai, R. K. et al. Development and initial validation of a deep learning algorithm to quantify histological features in colorectal carcinoma including tumour budding/poorly differentiated clusters. *Histopathology* **79**, 391–405 (2021).

Acknowledgements

Author contributions

Funding

Declarations

Competing interests

Additional information

Supplementary Information The online version contains supplementary material available at https://doi.org/10.1038/s41598-025-00866-x.

Correspondence and requests for materials should be addressed to T.S.H. or I.N.

Reprints and permissions information is available at www.nature.com/reprints.

Publisher's note Springer Nature remains neutral with regard to jurisdictional claims in published maps and institutional affiliations.